This is a repository copy of *Multi-Mode Modelling of a Flexible Link Robot Mnaipulator*.

White Rose Research Online URL for this paper:
http://eprints.whiterose.ac.uk/79934/

Monograph:

Morris, A.S. and Madani, A. (1995) Multi-Mode Modelling of a Flexible Link Robot Mnaipulator. Research Report. ACSE Research Report 579 . Department of Automatic Control and Systems Engineering

---

Departm

**AUTOMATIC
CONTROL
and SYSTEMS
ENGINEERING**
UNIVERSITY of SHEFFIELD
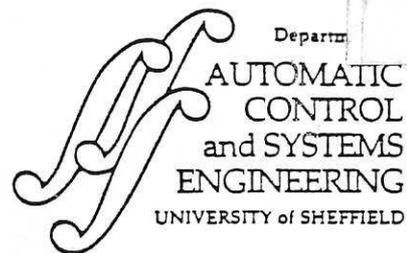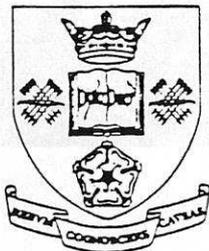
MULTI-MODE MODELLING OF A FLEXIBLE LINK ROBOT MANIPULATOR

A. S. MORRIS and A. MADANI

Robotics Research Group,

Department of Automatic Control and Systems Engineering,

The University of Sheffield, Mappin Street, Sheffield, S1 3JD, United Kingdom.

MULTI-MODE MODELING OF A FLEXIBLE LINK ROBOT MANIPULATOR

by

A. S. Morris, B.Eng, PhD, CEng, MIEE, MInstMc and A. Madani, B.Eng

ABSTRACT

This paper is addressed towards the problem of developing an accurate static and dynamic model for a two-flexible-link manipulator. The inadequacy of existing techniques for flexible link modeling is explained and a new formulation, based on an assumed mode modeling technique with a correction factor derived from finite element analysis, is derived. This takes account of second and third modes in the dynamics and is shown to provide an improvement in model accuracy compared with most existing modeling algorithms which neglect these higher modes.

1 Introduction

The control difficulties arising out of the use of large mass, high inertia links in conventional robot manipulators have been long recognised, and there has been much research activity directed towards developing robots with lightweight links. However, this in turn introduces a different control problem in respect of the elastic deflection and oscillatory behaviour due to the inherent flexibility of lightweight links.

Study of a typical six-degree-of-freedom, revolute geometry robot used in industry reveals that only two links contribute significantly to the inertia problem, and therefore only these two links have to be replaced by lightweight (and flexible) ones in order to address the inertia problem. Thus a suitable mechanism for developing a control strategy for such a modified robot is to study the characteristics of a two-flexible-link system and to superimpose the equations of additional rigid links on top of this.

A suitable approach towards developing the model necessary for analysing the two-link system is to model the motion of each link separately and then to examine how these separate models can be combined together so that the coupling between the links is properly described. With regard to the single-link modelling problem, much research has already been carried out and reported. However, most of this research has been concerned only with vibrations in the link rather than with the rotational motion of the link about its actuated joint (as occurs in a real manipulator). Even where rotational motion has been modelled, the single link models derived have insufficient accuracy for use in a two-link system, where the flexure and oscillations of the first link are transmitted to the second link and any modelling errors are cumulative.

This paper describes the development of a single-flexible-link model which avoids the simplifications and approximations made in previous work, in particular by including modes which other authors have neglected, and so yields a model of adequate accuracy. Following further work, the development of the single link models into a composite two-link dynamic model will be reported in a future paper.

2 Model Formulation

The basic equations describing the motion of a flexible link are highly nonlinear and thus are difficult and costly to compute. A more efficient formulation can be developed by using approaches such as Partial Differential Equations, the Assumed Mode technique or Finite Element Methods. These all have merits, but also disadvantages. For example, the Partial Differential Equation (PDE) approach gives the best description of the physical structure dynamics, but the solution is very difficult to obtain except for some very simple special cases where rotation is minimal or completely absent. The Assumed Mode Method (AMM) assumes the mode shape function of a system and provides a very computationally efficient scheme. Its disadvantage is that the real mode shape functions of a practical system are difficult to predict, especially for the case of robot manipulators where rigid motions are involved. The Finite Element Method (FEM) provides the best modeling capabilities among the three approaches. It can model a flexible structure with arbitrary link shapes and boundary conditions, but the convergence of its solution is not ideal because of the numerical approximations involved in the elaboration of the model. Whilst it simplifies the PDE model greatly, the computational burden is still very demanding.

The disadvantage of each of these approaches suggests that a better solution would be to use a combination of two or all three of these methods in order to exploit their advantages simultaneously and achieve an accurate but computationally efficient model. The formulation used therefore combines the assumed mode technique with finite element theory. The basis of the model is the Assumed Mode Method, but accuracy is improved by introducing a correcting factor derived from the finite element analysis.

3 Static Deflection of a Flexible link

Assuming the magnitude of flexure to be low, the slope and deflection of a flexible beam bending under gravity are described by:

$$\frac{du_m}{dx} = -\frac{mg}{2EIl}\left(l^2x - lx^2 + \frac{x^3}{3}\right) \quad ; \quad u_m = -\frac{mg}{2EIl}\left(\frac{l^2x^2}{2} - \frac{lx^3}{3} + \frac{x^4}{12}\right) \tag{1}$$

where m is the mass of the beam, l is the length of the beam, EI is the flexural stiffness of the beam, g is the gravity vector, x is the position on the beam of the point where the slope and deflection is measured and the subscript m denotes the slope or deflection resulting from the mass of the beam.

For a flexible link with an end-tip load m_t (Fig. 4-1), the mass m_t produces a negative slope and deflection given by:

$$\frac{du_{m_t}}{dx} = -\frac{m_t g}{EI}\left(lx - \frac{x^2}{2}\right) \quad ; \quad u_{m_t} = -\frac{m_t g}{EI}\left(\frac{lx^2}{2} - \frac{x^3}{6}\right) \tag{2}$$

By the principle of superposition the total static slope and deflection for a flexible link are given by:

$$\frac{du}{dx} = \frac{du_m}{dx} + \frac{du_{m_t}}{dx} = -\frac{g}{2EIl}\left((m + 2m_t)l^2x - (m + m_t)lx^2 + \frac{mx^3}{3}\right)$$

$$u = u_m + u_{m_t} = -\frac{g}{2EIl}\left((m + 2m_t)\frac{l^2x^2}{2} - (m + m_t)\frac{lx^3}{3} + \frac{mx^4}{12}\right) \tag{3}$$

The maximum static slope and deflection of the flexible link occur at the free end, where $x = l$, i.e.

$$\frac{du_{max}}{dx} = -\frac{l^2g}{2EI}\left(\frac{m}{3} + m_t\right) \quad ; \quad u_{max} = -\frac{l^3g}{2EI}\left(\frac{m}{4} + \frac{2m_t}{3}\right) \tag{4}$$

Unfortunately, if the assumption of low magnitude flexure is violated, Eqs. (1) to (4) are no longer valid and a correction factor is needed, as explained below.

4 Correction Factor

In Fig. 1 and Eqs. (1) to (4), the slope (and the deflection) of the link are calculated at a distance x from the origin of the link. The deflection is calculated at a distance perpendicular to the horizontal axis which is valid if the curvature (slope) of the link is very small. If the slope is greater than 5 degrees, the length of the bent link becomes greater than it should be. The correcting factor introduced uses finite element theory and results in a more accurate representation of the flexible link, as seen in Fig. 2 for a three-element link representation.

Suppose that the link is divided into n equal elements. For the first element, we have $i = 1$ and

$$u(l/n, t) = -\frac{g}{2EIl}\left((m + 2m_t)\frac{l^2(l/n)^2}{2} - (m + m_t)\frac{l(l/n)^3}{3} + \frac{m(l/n)^4}{12}\right) \tag{5}$$

This deflection, being at the distance $x = l/n$ on the OX axis, is actually greater than the real one since the element conserves its length l/n. When subject to the deflection, element 1 is rotated about its origin, an extra length v_1 is added to the element and the deflection is taken from a distance shorter than l/n by w_1, where v_1 and w_1 are given by:

$$v_1 = \sqrt{u(l/n, t)^2 + (l/n)^2} - l/n \quad ; \quad w_1 = \frac{v_1 l}{n\sqrt{u(l/n, t)^2 + (l/n)^2}} \tag{6}$$

2

So the corrected deflection at the point $x = l/n$ is given by:

$$u(l/n - s, t) = \frac{w_1}{v_1} \, u(l/n, t) \tag{7}$$

with s being an accumulative coefficient equal to w_1 for the first element. This coefficient corrects the distance at which the deflection is taken on the OX axis. It will obviously increase with the following elements. For the second element ($i = 2$), the deflection is first taken from a distance $x = (l/n - s) + l/n = 2l/n - s$,

$$u(2l/n - s, t) = - \frac{g}{2EIl} \left((m + 2m_t) \frac{l^2(2l/n - s)^2}{2} \right) + \frac{g}{2EIl} \left((m + m_t) \frac{l(2l/n - s)^3}{3} \right)$$
$$- \frac{g}{2EIl} \left(\frac{m(2l/n - s)^4}{12} \right) \tag{8}$$

The extra length added to the second element is v_2 and the reduction when projected onto the horizontal axis is w_2, where:

$$v_2 = \sqrt{\left(u(2l/n - s, t) - u(l/n - s, t) \right)^2 + (l/n)^2} - l/n$$

$$w_2 = \frac{v_2 l}{n\sqrt{\left(u(2l/n - s, t) - u(l/n - s, t) \right)^2 + (l/n)^2}} \tag{9}$$

So the corrected deflection at $x = 2l/n - s$ becomes

$$u(2l/n - s - w_2, t) = \frac{w_2}{v_2} \, u(2l/n - s, t) \tag{10}$$

s is then increased by w_2 (i.e., $s = w_1 + w_2$). Similar operations are carried out on the following elements, resulting in the equations below for the final element:

$$s = \sum_{i=1}^{n-1} w_i \tag{11}$$

$$v_n = L - l/n \; ; \qquad w_n = \frac{v_n l}{nL} \; ; \qquad L = \sqrt{\left(u(l - s, t) - u((n-1)l/n - s, t) \right)^2 + (l/n)^2} \tag{12}$$

$$u(l - s - w_n, t) = \frac{w_n}{v_n} \, u(l - s, t) \tag{13}$$

It is apparent that the true end-tip deflection is smaller than the one predicted by Eq. (4), and the slope is consequently reduced in a like manner. The projection of the end-tip of the deflected link on the horizontal axis is now equal to $l - \sum_{i=1}^{n} w_i$ and not l, proving that the position of the end-tip is not $(l, u(l, t))$ but $(l - s, u(l - s, t))$.

5   Free Vibration of a Flexible Link

A dynamic system can be set into motion either by some *initial conditions* or by disturbances at time zero. If no disturbance or excitation is applied after time zero, the oscillatory motions of the system are called *free vibrations*. Hence free vibrations describe the natural behaviour or the *natural modes* of vibration of the system. The initial condition is an energy input initially stored in the system.

If the system does not possess damping, there is no energy dissipation and the initial conditions will cause the vibrations to maintain themselves without any decrease in amplitude. However with damping, energy will be dissipated in the damper and the free vibrations will eventually die out, causing the system to regain its static equilibrium position.

3

5.1 Undamped Case

The equation of motion of an undamped flexible link without payload is described by [S. Timoshenko et al., 1974; R. H. Cannon, 1984]:

$$\rho \frac{\partial^2 u(x,t)}{\partial t^2} = -\frac{\partial^2}{\partial x^2}\left(EI\frac{\partial^2 u(x,t)}{\partial x^2}\right) ; \qquad u(x,t) = \phi(x)q(t) \tag{14}$$

where ρ is the mass per unit length of the link, $u(x,t)$ is the deflection of the link, $\phi(x)$ is the assumed mode shape function and $q(t)$ is the modal function. Assuming that EI is a constant, allows Eq. (14) to be written as

$$\frac{1}{q(t)}\frac{d^2 q(t)}{dt^2} = -\frac{EI}{\rho}\frac{1}{\phi(x)}\frac{d^4\phi(x)}{dx^4} \tag{15}$$

which leads to the two following differential equations:

$$\frac{d^4\phi(x)}{dx^4} - \beta^4\phi(x) = 0 ; \qquad \frac{d^2 q(t)}{dt^2} + \omega^2 q(t) = 0 \tag{16}$$

where w is a constant and $\beta^4 = \rho\omega^2/EI$.

The solution in [S. Timoshenko et al., 1974; R. H. Cannon, 1984]:

$$\phi_i(x) = C_i(\cos\beta_i x - \cosh\beta_i x) + (\sin\beta_i x - \sinh\beta_i x) \tag{17}$$

and

$$q_i(t) = A_i\cos\omega_i t + B_i\sin\omega_i t \tag{18}$$

where A_i, B_i, C_i and ω_i are constants, i denotes the number of modes of vibration. The deflection is then given by

$$u(x,t) = \sum_{i=1}^{\infty}\phi_i(x)q_i(t) \tag{19}$$

From the boundary conditions $(u(0,t) = u(l,t) = \frac{\partial u}{\partial x}(0,t) = \frac{\partial^2 u}{\partial x^2}(l,t) = 0)$ we obtain

$$C_i = \frac{\cos\ \beta_i l + \cosh\ \beta_i l}{\sin\ \beta_i l - \sinh\ \beta_i l} \tag{20}$$

and β_i as a solution to

$$\cos\ \beta_i l\ \cosh\ \beta_i l = -1 \tag{21}$$

Solving Eq. (21) for the first four modes gives $\beta_1 l = 1.875$, $\beta_2 l = 4.694$, $\beta_3 l = 7.854$ and $\beta_4 l = 10.995$. From here, using the definition that $\beta_i^4 = \rho\omega_i^2/EI$, we can deduce the values of the natural frequencies ω_i of the flexible link for the first four modes. This means that, given an initial excitation F, the link is going to oscillate according to a combination of these four natural frequencies.

The equation of motion can be generalised as an eigenvalue problem linking the two parts of the system (the assumed mode shape functions $\phi_i(x)$ and the modal functions $q_i(t)$).
Let the partial differential equations of the link be generalised as

$$P(\ddot{u}) + Q(u) = 0 \tag{22}$$

where P and Q are linear differential operators involving only the variable $x^\dagger$. So P, for example, will have the form

$$P = a_0 + a_1\frac{\partial}{\partial x} + a_2\frac{\partial^2}{\partial x^2} + \dots \quad \text{leading to} \quad P(u) = a_0 u + a_1\frac{\partial u}{\partial x} + a_2\frac{\partial^2 u}{\partial x^2} + \dots$$

The displacement u is as defined in Eq. (14), that is, $u(x,t) = \phi(x)q(t)$, and substituting this in Eq. (22) and simplifying, we obtain

$$\frac{P(\phi)}{Q(\phi)} = -\frac{\ddot{q}}{q} = \lambda \tag{23}$$

---

†For simplicity, the symbol (˙) denotes the partial differentiation with respect to time and (ʹ) with respect to the space variable x.

4

where λ is a constant, since $P(\phi)/Q(\phi)$ is a function of x and $\ddot{q}/q$ is a function of t. Thus,

$$\ddot{q} + \lambda q = 0 \; ; \qquad P(\phi) = \lambda Q(\phi) \tag{24}$$

The eigenvalue problem formulation of continuous systems is as shown in the above equation, where λ is an eigenvalue and $\phi(x)$ an eigenfunction. The problem is to find the values of λ for which there are functions $\phi(x)$ satisfying Eq. (24) and the boundary conditions. The forms of P and Q depend on the type of beam the link is made of. For most problems, Q is merely a weighting factor but becomes a constant for a uniform link. P is illustrated in Eq. (14) as being

$$P = \frac{\partial^2}{\partial x^2}\left(EI\frac{\partial^2}{\partial x^2}\right) \tag{25}$$

The boundary conditions are of the form $R(\phi) = \lambda S(\phi)$, where R and S are linear differential operators involving the space variable x only. The right side of the equation is obtained from the inertia term by replacing $\partial^2 u/\partial t^2$ by $-\lambda u$. Hence if the end-tip has no mass attached to it, we get $R(\phi) = 0$. In other words, the eigenvalue λ will appear in the boundary conditions only if the system has a payload at its end-tip. The orthogonality of the eigenfunctions can be demonstrated as follows:

From Eq. (24), for the rth and sth modes, we have

$$P(\phi_r) = \lambda_r Q(\phi_r) \quad \text{or} \quad \phi_s P(\phi_r) = \lambda_r \phi_s Q(\phi_r)$$

and

$$P(\phi_s) = \lambda_s Q(\phi_s) \quad \text{or} \quad \phi_r P(\phi_s) = \lambda_s \phi_r Q(\phi_s) \tag{26}$$

Substituting one equation for the other and integrating over the domain Σ of the elastic body, we obtain

$$\int_\Sigma [\phi_s P(\phi_r) - \phi_r P(\phi_s)]d\sigma = \int_\Sigma [\lambda_r \phi_s Q(\phi_r) - \lambda_s \phi_r Q(\phi_s)]d\sigma \tag{27}$$

If the eigenvalues are distinct and the eigenfunctions are selfadjoint, i.e.,

$$\int_\Sigma \phi_r P(\phi_s)d\sigma = \int_\Sigma \phi_s P(\phi_r)d\sigma \tag{28}$$

and

$$\int_\Sigma \phi_r Q(\phi_s)d\sigma = \int_\Sigma \phi_s Q(\phi_r)d\sigma \tag{29}$$

this results in the left-hand side of Eq. (27) being equal to zero, that is,

$$\int_\Sigma [\phi_s P(\phi_r) - \phi_r P(\phi_s)]d\sigma = 0 \tag{30}$$

and

$$\int_\Sigma [\lambda_r \phi_s Q(\phi_r) - \lambda_s \phi_r Q(\phi_s)]d\sigma = (\lambda_r - \lambda_s)\int_\Sigma \phi_r Q(\phi_s)d\sigma = 0 \tag{31}$$

Since $\lambda_r \neq \lambda_s$, we deduce that

$$\int_\Sigma \phi_r Q(\phi_s)d\sigma = 0 \quad \text{for} \quad r \neq s \tag{32}$$

Similarly, it can be shown that

$$\int_\Sigma \phi_r P(\phi_s)d\sigma = 0 \quad \text{for} \quad r \neq s \tag{33}$$

The last two equations prove that the eigenfunctions possess orthogonal properties and therefore are linearly independent from one another.

Substituting Eq. (25) in (33) and then integrating by parts, we obtain

$$
\begin{aligned}
\int_0^l [\phi_r(EI\phi_s'')'' - \phi_s(EI\phi_r'')'']dx &= \left\{ [\phi_r(EI\phi_s'')']_0^l - \int_0^l \phi_r'(EI\phi_s'')'dx \right\} \\
&\quad - \left\{ [\phi_s(EI\phi_r'')']_0^l - \int_0^l \phi_s'(EI\phi_r'')'dx \right\} \\
&= \left\{ [\phi_r(EI\phi_s'')' - \phi_r'(EI\phi_s'')]_0^l + \int_0^l EI\phi_r''\phi_s''dx \right\} \\
&\quad - \left\{ [\phi_s(EI\phi_r'')' - \phi_s'(EI\phi_r'')]_0^l + \int_0^l EI\phi_s''\phi_r''dx \right\} \\
&= [\phi_r(EI\phi_s'')' - \phi_s(EI\phi_r'')']_0^l \\
&\quad - [\phi_r'EI\phi_s'' - \phi_s'EI\phi_r'']_0^l
\end{aligned}
\tag{34}
$$

The eigenfunctions being selfadjoint, Eq. (34) is identically zero if the boundary conditions at each end can be expressed as

$$
a\phi + b(EI\phi'')' = 0 ; \qquad c\phi' + d(EI\phi'') = 0
\tag{35}
$$

The constants a, b, c and d depend on the boundary conditions of the link. The orthogonal relations in Eqs. (32) and (33) become

$$
\int_0^l \rho l\phi_r\phi_s dx = \begin{cases} 0 & \text{for } r \neq s \\ m_{rr} & \text{for } r = s \end{cases}
\tag{36}
$$

where m_{rr} is the normalised mass of the system for the rth mode.
And

$$
\int_0^l EI\phi_r''\phi_s'' dx = \begin{cases} 0 & \text{for } r \neq s \\ k_{rr} & \text{for } r = s \end{cases}
\tag{37}
$$

where k_{rr} is the normalised flexural stiffness of the system for the rth mode. From here, it can be deduced that the natural frequencies of the link are $\omega_i = \sqrt{k_{ii}/m_{ii}}$, with i being the mode order. Considering the case of the first mode as an example, we have

$$
\phi_1(x) = C_1(\cos \beta_1 x - \cosh \beta_1 x) + (\sin \beta_1 x - \sinh \beta_1 x)
$$

where

$$
C_1 = (\cos \beta_1 l + \cosh \beta_1 l)/(\sin \beta_1 l - \sinh \beta_1 l)
$$

The calculated value for C_1 is -1.3622, since $\beta_1 l = 1.875$. Thus,

$$
\begin{aligned}
m_{11} &= \int_0^l \rho l\phi_1^2(x)dx = \left(\frac{\rho l}{\beta_1}\right) \int_0^{\beta_1 l} \phi_1^2(x)d\beta_1 x \\
&= \left(\frac{\rho l}{\beta_1}\right) \int_0^{\beta_1 l} [C_1(\cos \beta_1 x - \cosh \beta_1 x) + (\sin \beta_1 x - \sinh \beta_1 x)]^2 d\beta_1 x \\
&= \left(\frac{\rho l}{\beta_1}\right) [C_1^2(4.8155) + 2C_1(2.4865) + (1.3181)] \\
&= 3.4795\rho l/\beta_1
\end{aligned}
\tag{38}
$$

And since

$$
\phi_i''(x) = -C_1\beta_i^2(\cos \beta_i x + \cosh \beta_i x) - \beta_i^2(\sin \beta_i x + \sinh \beta_i x)
$$

we get for the normalised stiffness[‡]

$$
k_{11} = EI\beta_1^3(17.2120 - 23.3269 + 9.5944) = 3.4795EI\beta_1^3
$$

giving

$$
\omega_1^2 = k_{11}/m_{11} = EI\beta_1^4/\rho l
$$

[‡] $\int (\phi_i'''')\phi_i dx = \int (\phi_i'')^2 dx$, and $d^4\phi_i/dx^4 = \beta_i^4\phi_i$.

5.1.1 Initial Conditions

Consider the deflection $u(x,t)$ of a flexible link given by Eq. (19). The initial conditions can be expressed as

$$u(x,0) = \sum_{i=1}^{\infty} \phi_i(x)q_i(0) = f(x) \ ; \qquad \dot{u}(x,0) = \sum_{i=1}^{\infty} \phi_i(x)\dot{q}_i(0) = g(x) \tag{39}$$

Using the orthogonal relation, the corresponding initial conditions in the *normal coordinates* (the normalisation or weighting is operated on all modes) are

$$q_i(0) = \frac{\rho l}{m_{ii}} \int_0^l f(x)\phi_i(x)dx \ ; \qquad \dot{q}_i(0) = \frac{\rho l}{m_{ii}} \int_0^l g(x)\phi_i(x)dx \tag{40}$$

Similarly, $q_i(0)$ and $\dot{q}_i(0)$ can be obtained from the normalised flexural stiffness as

$$q_i(0) = \frac{EI}{k_{ii}} \int_0^l f''(x)\phi_i''(x)dx \ ; \qquad \dot{q}_i(0) = \frac{EI}{k_{ii}} \int_0^l g''(x)\phi_i''(x)dx \tag{41}$$

So, if the link is submitted to an initial displacement due to a force F applied to the end-tip, this displacement can be written as follows

$$f(x) = -\frac{F}{EI}\left(\frac{lx^2}{2} - \frac{x^3}{6}\right) \tag{42}$$

and its effect is to force the undamped link to vibrate according to its natural frequencies.
The first and second derivatives of $f(x)$ with respect of the space variable x are

$$f'(x) = -\frac{F}{EI}\left(lx - \frac{x^2}{2}\right) \quad \text{and} \quad f''(x) = -\frac{F}{EI}(l - x)$$

Knowing from Eqs. (17) to (20) that the equation of motion of an undamped flexible link can be formulated as

$$u(x,t) = \sum_{i=1}^{\infty} \phi_i(x)q_i(t)$$

where

$$\phi_i(x) = C_i(\cos\beta_i x - \cosh\beta_i x) + (\sin\beta_i(x) - \sinh\beta_i x)$$
$$q_i(t) = A_i \cos\omega_i t + B_i \sin\omega_i t$$

we can deduce from the initial conditions that $B_i = 0$ and, by analogy to Eq. (39), $A_i = q_i(0)$.
The following functions can be obtained from $\phi_i(x)$:

$$\phi_i' = -C_i\beta_i(\sin\beta_i x + \sinh\beta_i x) + \beta_i(\cos\beta_i - \cosh\beta_i)$$
$$\phi_i'' = -C_i\beta_i^2(\cos\beta_i x + \cosh\beta_i x) - \beta_i^2(\sin\beta_i + \sinh\beta_i) \tag{43}$$

C_i can be obtained from Eq. (20) and values of $q_i(0)$ can be obtained from Eq. (41):

$$
\begin{aligned}
q_i(0) &= \frac{Fl\beta_i^2}{k_{ii}} \int_0^l [C_i(\cos\beta_i x + \cosh\beta_i x) + (\sin\beta_i x + \sinh\beta_i x)]dx \\
&\quad - \frac{F\beta_i^2}{k_{ii}} \int_0^l [C_i(x\cos\beta_i x + x\cosh\beta_i x) + (x\sin\beta_i x + x\sinh\beta_i x)]dx \\
&= \frac{FlC_i\beta_i}{k_{ii}}[\sin\beta_i x + \sinh\beta_i x]_0^l + \frac{Fl\beta_i}{k_{ii}}[-\cos\beta_i x + \cosh\beta_i x]_0^l \\
&\quad - \frac{FC_i\beta_i}{k_{ii}}\left[x\sin\beta_i x + \frac{1}{\beta_i}\cos\beta_i x + x\sinh\beta_i x - \frac{1}{\beta_i}\cosh\beta_i x\right]_0^l \\
&\quad - \frac{F\beta_i}{k_{ii}}\left[-x\cos\beta_i x + \frac{1}{\beta_i}\sin\beta_i x + x\cosh\beta_i x - \frac{1}{\beta_i}\sinh\beta_i x\right]_0^l \\
&= \frac{F}{k_{ii}}[C_i(\cosh\beta_i l - \cos\beta_i l) + (\sinh\beta_i l - \sin\beta_i l)] \\
&= -\frac{F}{k_{ii}}\phi_i(l) \tag{44}
\end{aligned}
$$

7

Taking into account the first three modes ($i =$1,2 and 3), equations can be obtained for the vertical displacement $u(x,t)$ of any point x on the link at any time t, the slope $u'(x,t)$ of the link at any point x and any time t and the velocity $\dot{u}(x,t)$ of any point x on the link at any time t:

$$u(x,t) = \phi_1(x)q_1(0)\cos\omega_1 t + \phi_2(x)q_2(0)\cos\omega_2 t + \phi_3(x)q_3(0)\cos\omega_3 t \tag{45}$$

$$u'(x,t) = \frac{\partial u(x,t)}{\partial x} = \phi_1'(x)q_1(0)\cos\omega_1 t + \phi_2'(x)q_2(0)\cos\omega_2 t + \phi_3'(x)q_3(0)\cos\omega_3 t \tag{46}$$

$$\dot{u}(x,t) = \frac{\partial u(x,t)}{\partial t} = -\phi_1(x)q_1(0)\omega_1\sin\omega_1 t - \phi_2(x)q_2(0)\omega_2\sin\omega_2 t - \phi_3(x)q_3(0)\omega_3\sin\omega_3 t \tag{47}$$

It is important to note that the natural frequencies $\omega_i = \sqrt{k_{ii}/m_{ii}}$ do not depend on the magnitude of the initial excitation force F but on the mass, length, width, flexural stiffness (characteristic of the material the link is made of) and the loading of the link.

Fig. 3 shows the free vibration of an undamped, unloaded, one-metre long flexible link for the first three modes of vibration with an excitation of 4 Newtons. The amplitude of the oscillations decreases enormously from one mode to another. In Fig. 4, the time history of the end tip displacement is compared for different initial excitation forces. The amplitude of the vibrations are proportional to the amplitude of the applied force F but the frequency of vibration remains a constant. This frequency increases of course for the higher modes, since β_i increases with i.

Figs. 3 and 4 show that the amplitude of the first mode is substantially greater than that of the other modes. Many researchers in this field have treated the amplitude of the higher modes as being negligible compared with that of the first mode, and have consequently ignored the higher modes in order to simplify the modeling task. However, study of Fig. 5 shows that the amplitude of the slope of the second mode is at least 10 percent of its counterpart in the first mode, and even in the third mode the amplitude of the slope is about 2 percent of that in the first mode. Thus these modes are significant and any simplification which neglects them is invalid.

These large slopes are confirmed by Figs. 3(b) and (c). The "sharpness" towards the end-tip proves that the amplitude of the slope (first derivative of the displacement with respect to the variable x) is very important. Also, the end-tip velocity (see Fig. 6) is seen to be relatively important at the third mode level (almost 5 percent of the amplitude of the end-tip velocity of the first mode). This proves once more the importance in choosing a sufficient number of modes in order to obtain a model for the flexible link with a high accuracy.

5.1.2 Addition of an End-Tip Load

If the system has an end-tip load, an eigenvalue λ (see Eqs. (23) to (24)) will appear in the boundary conditions. Under such conditions, the eigenfunctions in Eq. (36) will not be orthogonal. An orthogonal relation can be derived by redefining the mass distribution of the system. The mass m_a attached to the free end of the flexible link adds the following boundary condition to the set of known ones:

$$EI\frac{\partial^3 u(x,t)}{\partial x^3} = m_a\frac{\partial^2 u(x,t)}{\partial t^2} \tag{48}$$

Let m_a be an integral part of the link. Hence:

$$\text{Total mass} = \rho l + m_a \quad \text{or} \quad \rho_{\text{total system}} = \rho + m_a\delta(x-l)$$

Since m_a is a concentrated mass, its mass/length becomes a delta function[†] $m_a\delta(x-l)$. If m_a is part of the link, then the boundary conditions beyond m_a is that of a free end beam.

[†]Dirac's delta function is defined such that $\delta(x-l) = 0$ for $x \neq l$ and $\int_{-\infty}^{\infty}\delta(x-l)dx = 1$

Using $m(x) = \rho + m_a \delta(x - l)$, the orthogonal relation in Eq. (36) becomes

$$
\begin{aligned}
\int_0^l [\rho + m_a \delta(x - l)] \phi_r \phi_s \, dx &= \int_0^l \rho \phi_r \phi_s \, dx + m_a \phi_r(l) \phi_s(l) \\
&= \begin{cases} 0 & \text{for } r \neq s \\ m_{ii} & \text{for } r = s \end{cases}
\end{aligned}
\tag{49}
$$

Since the operator P in Eq. (33) is not affected by m_a, the corresponding orthogonal relation remains as shown in Eq. (37). An increase in m_{ii} will imply a decrease in ω_i and therefore, the link will vibrate in a slower manner when a load is attached to its free end, and vibrations will persist for a longer time.

Since the payload does not affect the value of k_{ii}, the quantity $q_i(0)$ can be obtained from Eq. (41). The frequency ω_i is then deduced as follows

$$
\omega_i = \sqrt{k_{ii}/m_{ii}}
$$

The new value of m_{ii} includes the mass of the payload m_a and therefore, the frequencies of vibration are decreased (or the period of vibration is increased).

Fig. 7 displays the free vibration of the first three modes around the static equilibrium position under the effect of a payload of 400g and various initial excitations. The amplitudes of vibration of the second and third modes are almost insignificant and at this level, the beam seems to be static. But, as seen in Fig. 8, their effect on the whole system is significant in terms of the slope and velocity.

It can be concluded that the initial conditions (here, the initial excitation force) only affect the amplitude of the vibration, and not the frequency. The payload, by contrast, operates on the frequency of the free vibration. The amplitude of vibration of the higher modes are negligible but the effect they have (especially the second mode) on the total slope and total velocity of the link cannot be ignored.

5.1.3 Application of the Correction Factor

Using the correction factor, it can be easily shown how the deflection, and specially the horizontal position, of any point on the link is obtained with more accuracy than that obtained from the assumed mode technique on its own. For this purpose, the flexible link is divided into 10 finite elements (see Fig. 9). This resulted in the appearance of two different vibrations: one in the vertical direction affecting the vertical position of the link, and one in the horizontal direction affecting the horizontal position of any point on the link. This second type of vibration cannot be described by classical theory equations for flexible beams, and only the finite element theory can help us in obtaining a realistic description of such vibrations. As a reminder, the excitation force responsible for the vibration is kept constant, causing the amplitude of the vibration to remain constant for different end-tip loads.

It can be easily seen, from Figs. 9(a), (b) and (c), how the length of the flexible link is corrected, causing the horizontal coordinate of any point on the link to be shifted towards the origin. This shift can be found to be as large as 100 mm for a link of 400 grammes with an end-tip of 400 grammes subject to an excitation force of 4 Newtons applied to the end-tip.

Consequently, the corrected deflection is slightly smaller (for both static equilibrium and total vibration) and is about 90 percent of the deflection obtained from the classical modeling method of the assumed mode technique. This improved accuracy is important in high precision robot manipulations.

5.2 Damped Case

When the dynamic system represented by the flexible link contains a damping process, the principal equation of motion shown in Eq. (14) becomes

$$\rho \frac{\partial^2 u(x,t)}{\partial t^2} + c \frac{\partial u(x,t)}{\partial t} = -\frac{\partial^2}{\partial x^2}\left(EI\frac{\partial^2 u(x,t)}{\partial x^2}\right) \tag{50}$$

where c is the damping coefficient of the link, which depends on the material the link is made of. This equation can be rewritten in the following form

$$\frac{c}{\rho}\frac{\partial u}{\partial t} + \frac{\partial^2 u}{\partial t^2} + a^2 \frac{\partial^4 u}{\partial x^4} = 0 \tag{51}$$

with $a^2 = EI/\rho$. So, assuming the modal representation of the deflection as in Eq. (14), we obtain

$$\frac{c}{\rho q}\frac{dq}{dt} + \frac{1}{q}\frac{d^2 q}{dt^2} = -a^2 \frac{1}{\phi}\frac{d^4 \phi}{dx^4} \tag{52}$$

The system of assumed mode shapes functions $\phi(x)$ remains unchanged (see Eqs. (16) and (17)), while the modal functions $q(t)$ become solutions to the following equation

$$\frac{d^2 q_i}{dt^2} + \frac{c}{m_{ii}}\frac{dq_i}{dt} + \omega_i^2 q_i = 0 \tag{53}$$

where $\omega_i = \sqrt{k_{ii}/m_{ii}}$ as discussed in the previous section.
The solution for such a differential equation is

$$q_i(t) = \exp^{-\frac{c}{2m_{ii}}t}(A_i \cos \omega_i^* t + B_i \sin \omega_i^* t) \tag{54}$$

where the frequency ω_i^* is equal to

$$\omega_i^* = \sqrt{\omega_i^2 - \frac{c^2}{4\rho^2}}$$

This means that the amplitude of the higher modes die out very quickly as shown in Fig. 10. The higher modes (modes 2 and 3) influence the total response of the system for only few fractions of a second, while the oscillation of the first mode persists longer. The damping coefficient decreases the vibrations of the flexible link and attenuates the effect of the high frequency modes. This must be taken into account in the modelling of a flexible link, since when the link is subject to some damping, its high frequency modes become no longer important in the dynamic response, except for the small fraction of time which follows the removal of the initial force. Fig. 11 shows the effect of varying the damping coefficient. A lower damping makes the amplitude of vibration decrease over a longer time period according to the relationship:

$$\frac{c}{2\rho}T = \ln \frac{Y_1}{Y_2}$$

where Y_1 is the value of the amplitude of the first peak, Y_2 is the value of the amplitude of the next peak and T the time period between these two consecutive peaks.

Fig. 12(a) shows the total end-tip deflection obtained from the three modes when the link is subject to damping. This total deflection is very slightly affected by the higher modes. In Fig. 12(b), the end-tip slope taken from the addition of the three slopes created by the modes is shown. The effect of the third mode is almost invisible while the effect of the second mode lasts only for 0.08 seconds. Fig. 12(c) shows that the corresponding end-tip velocity is due mainly to the first mode but proves that the second mode is operating during the first 0.12 seconds. Finally, Fig. 13 displays a three-dimensional representation of a loaded flexible link with and without damping.

10

Fig. 5 Free vibration of the end-tip slope for the first three modes and different excitations.

(c) Third mode.

End-tip slope in degrees
Time in seconds
F=4Newtons

(b) Second mode.

End-tip slope in degrees
Time in seconds
F=1Newton
F=4Newtons

(a) First mode.

End-tip slope in degrees
Time in seconds
F=1Newton
F=4Newtons

Fig. 3 Free vibration of a flexible link with no payload.
Mass of the link = 400g. Excitation = 4 Newtons.

(c) Third mode.

Vertical displacement in metres
Horizontal position in metres
$\times 10^{-3}$

(b) Second mode.

Vertical displacement in metres
Horizontal position in metres
$\times 10^{-3}$

(a) First mode.

Vertical displacement in metres
Horizontal position in metres

Fig. 4 Free vibration of the first three modes for initial excitations of 1,2,3 and 4 Newtons.

(c) Third mode.

Vertical displacement in metres
Time in seconds
F=4Newtons
$\times 10^{-3}$

(b) Second mode.

Vertical displacement in metres
Time in seconds
F=1Newton
F=4Newtons
$\times 10^{-3}$

(a) First mode.

Vertical displacement in metres
Time in seconds
F=1Newton
F=4Newtons

Fig. 2 Corrections to the deflection of a flexible link.
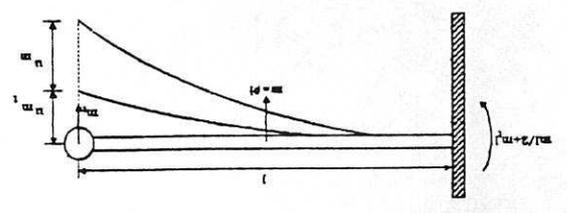
Fig. 1 Deflection of a flexible link under the effect of its mass and payload.
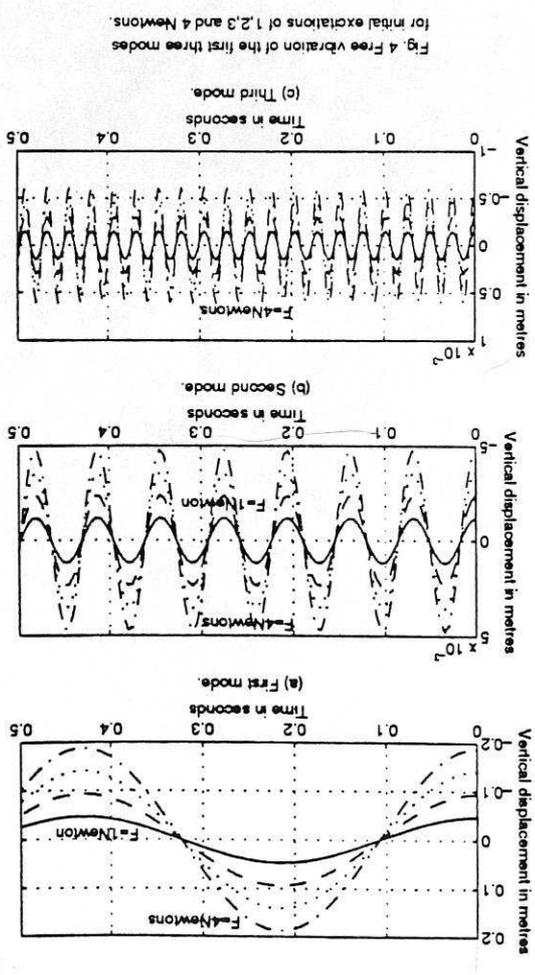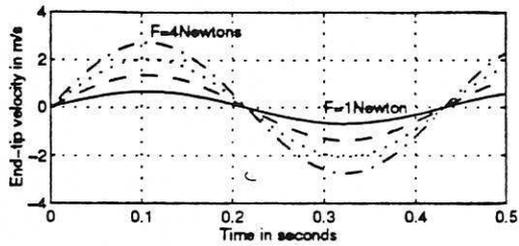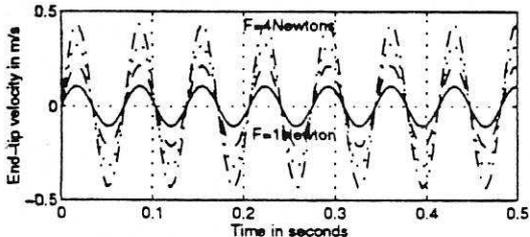
(a) First mode.
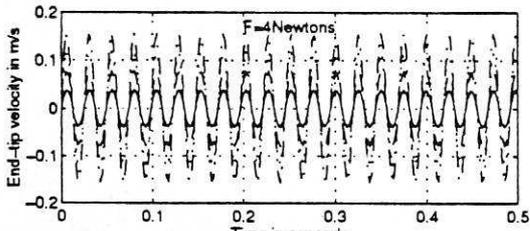
(b) Second mode.

(c) Third mode.

Fig. 6 End–tip velocity for the first three modes
for different initial excitations.

(a) Total deflection (superposition of 3 modes) for different excitations.

(b) Total slope (superposition of 3 modes) for different excitations.

(c) Total velocity (superposition of 3 modes) for different excitations.

Fig. 8 Free vibration around the static equilibrium position
for initial excitations of 1,2,3 and 4 Newtons. Payload = 400g.
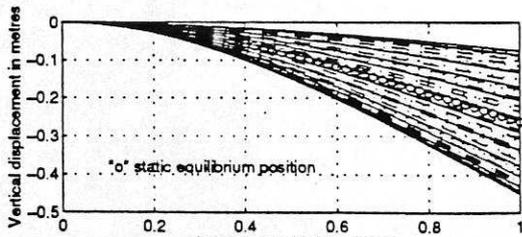
(a) First mode.
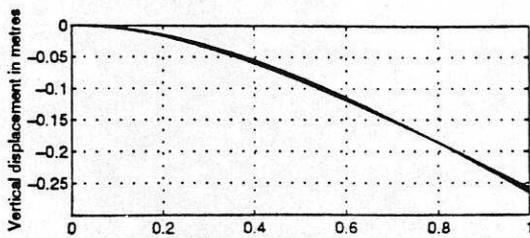
(b) Second mode.
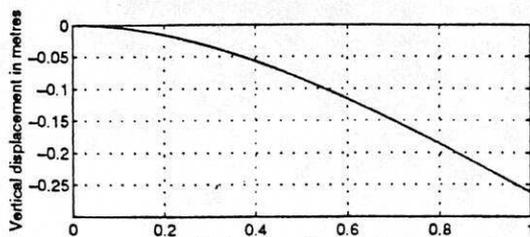
(c) Third mode.

Fig. 7 Free vibration of a flexible link around its static equilibrium position.
Mass of link = 400g. Excitation = 4 Newtons. Payload = 400g.
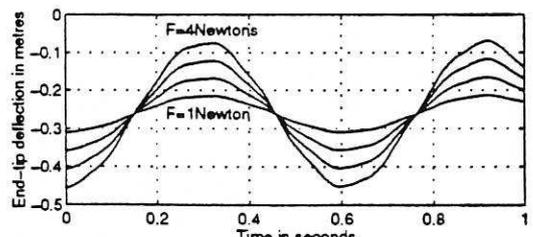
(a) Total deflection (superposition of 3 modes) for different excitations.

(b) Total slope (superposition of 3 modes) for different excitations.

(c) Total velocity (superposition of 3 modes) for different excitations.

Fig. 8 Free vibration around the static equilibrium position
for initial excitations of 1,2,3 and 4 Newtons. Payload = 400g.

(a) Mass of link = 400g. No payload.
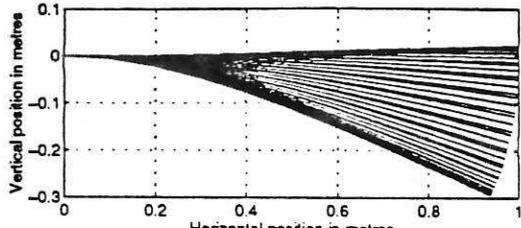
(b) Mass of link = 400g. Payload = 200g.
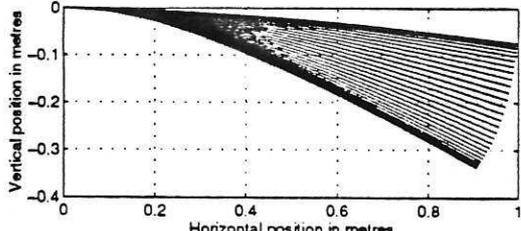
(c) Mass of link = 400g. Payload = 400g.

Fig. 9 Free vibration of a flexible link using the correcting factor method.
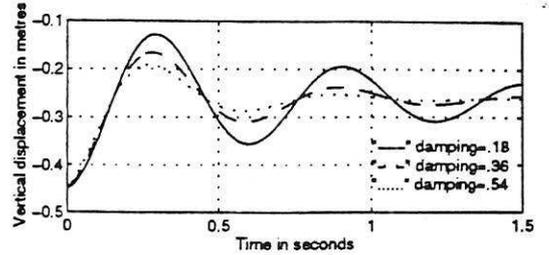
(a) First mode.
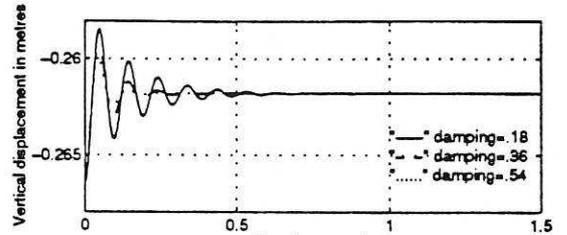
(b) Second mode.
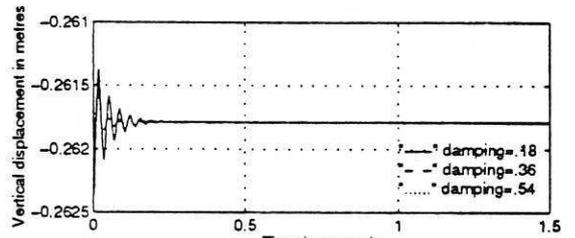
(c) Third mode.

Fig. 11 Damped free vibration of the first three modes
for different damping factors. F = 4Newtons. Payload = 400g.
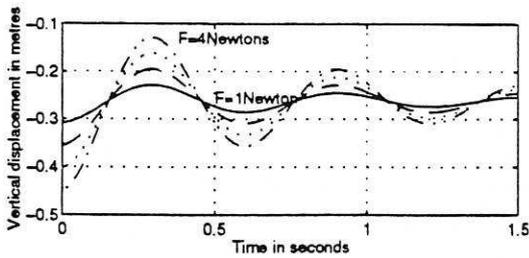
(a) First mode.
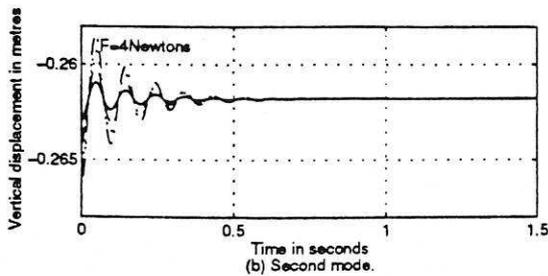
(b) Second mode.
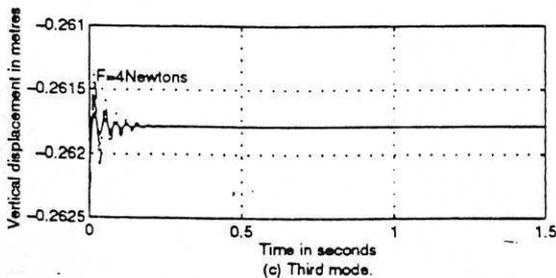
(c) Third mode.

Fig. 10 Damped free vibration of the first three modes
for initial excitations of 1,2,3 and 4 Newtons. Payload = 400g.
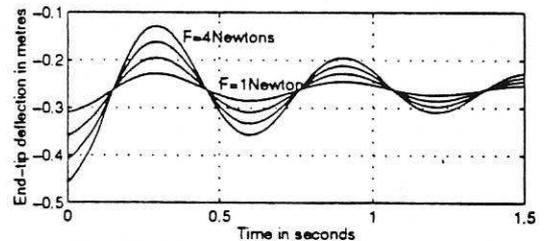
(a) Total deflection (superposition of 3 modes) for different excitations.
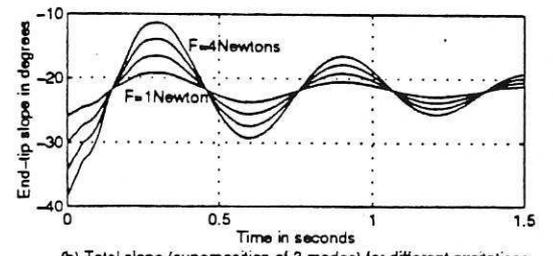
(b) Total slope (superposition of 3 modes) for different excitations.
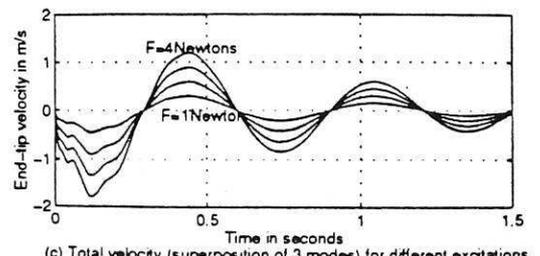
(c) Total velocity (superposition of 3 modes) for different excitations.

Fig. 12 Damped free vibration around the static equilibrium position
for initial excitations of 1,2,3 and 4 Newtons. Payload = 400g.
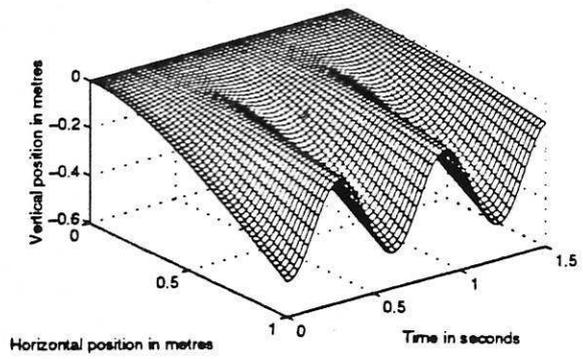
Fig. 13(a) Undamped free vibration of a link. Payload = 400g.
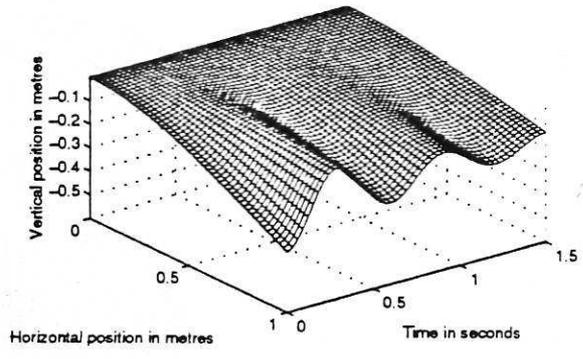
Fig. 13(b) Damped free vibration of a link. Payload = 400g.

6 Summary

In this work, the static bending of a flexible link under its own mass and then under the effect of end-tip loading has been studied. The classical theory for flexible beams has been proven incapable of predicting the exact position of any point of the link. For this reason, a correction based on finite elements theory has been incorporated. The results obtained by using this method have been shown to improve accuracy and to give a more realistic description of what really happens to a flexible link. The length of the link cannot in any circumstances change, and therefore the real horizontal position is not as predicted by classical theory of beams.

Then, the subject of free vibrations has been treated, starting with an undamped flexible link to show how its natural frequencies affect the motion of the dynamic system. Different initial excitations have been used as an input to the system to prove that these natural frequencies cannot be affected by the initial conditions. It has also been demonstrated how the end-tip load affects the speed of vibration of the link. An unloaded flexible link will vibrate faster than a heavily loaded one.

In this work, the general influence that the high modes have on the system has been shown. It has been proven that, even if the amplitude of vibration of the second mode is negligible in comparison with the amplitude of the first mode, the corresponding slope and velocity play an important role in the total response of the system. The high frequency oscillations due to the second mode make the link appear to be motionless, but the slope created at the end-tip, especially, adds enormously to the slope created by the first slower mode. Accurate modeling of flexible links must therefore involve at least the first two modes.

Finally, the system consisting of the link and its end-tip load has been studied with the additional effect of a damping coefficient. This damping, created by the link's material itself, decreased both the amplitude and natural frequencies of the vibrations. The link was first subject to some oscillations which died out after a certain period of time dictated by the damping coefficient, and then stablised at the static equilibrium position. The importance of the second mode has been proven once more, but its effect lasted only a small fraction of time.

References

S. Timoshenko, D. H. Young, and W. Weaver, Jr., *Vibration Problems in Engineering*. New York: Wiley, 1974.

R. H. Cannon, Jr. and E. Schmitz, "Initial experiments on the end-point control of a flexible one-link robot." *Int. J. Robotics Res.*, vol. 3, no. 3, pp. 62-75, 1984.